

Crystallographic Texture of Stress–Affected Bainite

BY SAURABH KUNDU, K. HASE AND H. K. D. H. BHADESHIA

*University of Cambridge
Materials Science and Metallurgy
Pembroke Street, Cambridge CB2 3QZ, U. K.
hkdb@cam.ac.uk, www.msm.cam.ac.uk/phase-trans*

1. Abstract

A method is presented for calculating both the macroscopic strains and crystallographic bias which develop when a polycrystalline sample of austenitic steel is transformed into bainite or martensite under the influence of an applied stress or a system of stresses. Any texture present in the austenite prior to transformation is taken into account, as is the detailed crystallography of the transformation. Comparisons with experimental data are encouraging. A strong correlation has been observed between the proportion of the driving force for transformation that is attributed to stress, and the extent of variant selection.

2. Introduction

Crystallographic texture is said to exist when a polycrystalline material has a non-random distribution of crystal orientations relative to the sample axes. This phenomenon is of particular importance in the processing and properties of steels. Texture can arise in many ways but the topic of interest here is that which develops as a consequence of the displacive transformation of austenite. There have been previous studies on the calculation of textures in these circumstances, but as pointed out in some recent work (Kundu and Bhadeshia, 2006), they involve a variety of assumptions which prevent rigorous predictions.

The method employed here is to use crystallographic data which are justified by the theory of martensite. This theory explains in a consistent manner, all the observed features of the martensite and related transformations (Bowles and MacKenzie, 1954; Wechsler et al., 1953). The second step is to calculate the interaction between the transformation product and the externally applied system of stresses. It is this interaction which leads to the development of texture because the stress favours the growth of particular crystallographic variants which comply with the applied stress (Patel and Cohen, 1953).

That the combination of crystallographic theory and interaction energy calculations in this manner can reliably predict the overall texture due to martensitic transformation has been demonstrated for austenitic stainless steel deformed in tension (Kundu and Bhadeshia, 2006). In the present work we investigate the microtexture that develops when individual grains of austenite transform into bainite.

The work presented in this paper is inspired by attempts to design welding alloys which counter the build up of residual stresses in welded joints (Bhadeshia, 2005a; Eckerlid et al., 2003; Ohta et al., 2003, 1999a,b). The strains caused by displacive phase transformations are manipulated to cancel the thermal contraction as welded joints cool to ambient temperature. The technological benefit of doing this is to dramatically improve the fatigue performance of the joints (Ohta et al., 1999b). It would be useful therefore to be able not only to estimate the development of transformation texture, but also the anisotropic trans-

formation strains caused by the biased microstructure that develops under the influence of stress.

The paper therefore begins with the estimation of crystallographic texture, followed by the calculation transformation strains and experimental validation. Possible interactions between crystallographic variants are neglected, and it is assumed in the first part of the paper that all favoured variants form in equal fraction. However, we then introduce a thermodynamic concept which permits a better estimation of the extent of microstructural bias.

3. Crystallography

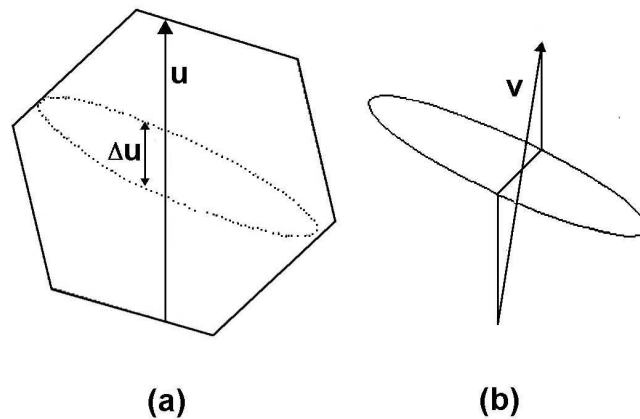


Figure 1. The deformation of an initial vector \mathbf{u} by the formation of bainite. (a) An austenite grain prior to transformation, with the ultimate location of a plate of bainite marked. (b) Following bainitic transformation.

Throughout this paper we use the vector and matrix notation due to Bowles and MacKenzie which is particularly good at avoiding confusion between frames of reference (Bhadeshia, 2001b; Bowles and MacKenzie, 1954). Consider a polycrystalline sample of austenite which is subjected to external stress. The sample axes are defined by an orthonormal set of basis vectors $[A; \mathbf{a}_1]$, $[A; \mathbf{a}_2]$ and $[A; \mathbf{a}_3]$, collectively identified using a basis symbol 'A'. The crystallographic axes of the i th austenite grain are similarly identified using the basis symbol F_i and its corresponding reciprocal basis by the symbol F_i^* .

When austenite transforms to bainite, there is a shape deformation which is an invariant-plane strain (Bhadeshia, 2001a; Ko and Cottrell, 1952; Swallow and Bhadeshia, 1996). This change in shape can be represented by a 3×3 deformation matrix \mathbf{P} such that:

$$(\mathbf{F} \mathbf{P} \mathbf{F}) = \mathbf{I} + m[\mathbf{F}; \mathbf{d}](\mathbf{p}; \mathbf{F}^*) \quad (3.1)$$

where m is the magnitude of the shape deformation, $[\mathbf{F}; \mathbf{d}]$ is a unit vector in the direction of displacement and $(\mathbf{p}; \mathbf{F}^*)$ is the unit normal to the invariant-plane (i.e., the habit plane). There will in general exist 24 crystallographic variants of bainite in any given austenite grain, i.e., 24 different invariant-plane strains.

Consider an arbitrary vector \mathbf{u} traversing a grain of austenite prior to transformation, as illustrated in Fig. 1a. This vector makes an intercept $\Delta\mathbf{u}$ with a domain of austenite that eventually ends up as a plate of bainite. As a consequence of the transformation, the vector \mathbf{u} becomes a new vector \mathbf{v} given by:

$$\mathbf{v} = \mathbf{P}\Delta\mathbf{u} + (\mathbf{u} - \Delta\mathbf{u}) \quad (3.2)$$

When considering the formation of large number of bainite plates in many austenite grains, \mathbf{u} traverses a polycrystalline sample of austenite so this equation must be generalised as follows:

$$\mathbf{v} = \sum_{k=1}^n \sum_{j=1}^{24} \mathbf{P}_j^k \Delta\mathbf{u}_j^k + \left(\mathbf{u} - \sum_{k=1}^n \sum_{j=1}^{24} \Delta\mathbf{u}_j^k \right) \quad (3.3)$$

where $j = 1 \dots 24$ represents the 24 crystallographic variants possible in each austenite grain, and $k = 1 \dots n$ represents the n austenite grains traversed by the vector \mathbf{u} . In this scenario of a large number of bainite plates, the intercepts $\Delta\mathbf{u}_j^k$ can be approximated by $f_j^k \mathbf{u}$ where f_j^k is the fraction of sample transformed by variant j in austenite grain k .

The deformation caused by a particular bainite plate j in austenite grain k , *i.e.*, $(\mathbf{F}_k \mathbf{P}_j \mathbf{F}_k) \equiv \mathbf{P}_j^k$ is known from the crystallographic theory originally developed for martensite (Bowles and MacKenzie, 1954; Wechsler et al., 1953). The remaining 23 such matrices for grain 1 of austenite can be deduced from this using symmetry operations. They can then be expressed in the reference frame of the sample using a similarity transformation as follows:

$$(\mathbf{S} \mathbf{P}_j^k \mathbf{S}) = (\mathbf{S} \mathbf{R} \mathbf{F}_k)(\mathbf{F}_k \mathbf{P}_j \mathbf{F}_k)(\mathbf{F}_k \mathbf{R} \mathbf{S}) \quad (3.4)$$

where $(\mathbf{S} \mathbf{R} \mathbf{F}_k)$ is the rotation matrix relating the basis vectors of the k th austenite grain to the sample axes, and $(\mathbf{F}_k \mathbf{R} \mathbf{S})$ is the inverse of that rotation matrix. In this way, the calculation described in equation 3.2 can be conducted in the sample frame of reference.

4. Variant Selection

Variant selection occurs because the shape deformation of a martensite or bainite plate may or may not comply with an external stress. Following Patel and Cohen (1953), the compliance of a particular variant with the applied stress can be expressed in terms of an interaction energy:

$$U = \sigma_N \zeta + \tau s \quad (4.1)$$

where σ_N is the stress component normal to the habit plane, τ is the shear stress resolved on the habit plane in the direction of shear and ζ and s are the respective normal and shear strains associated with transformation.

The applied system of stresses can be described by a 3×3 stress tensor σ_{lm} which when multiplied by the unit normal to the bainite habit plane gives the traction \mathbf{t} describing the state of stress on that plane. The traction can then be resolved into σ_N and τ in the normal manner (Timoshenko and Goodier, 1982):

$$\begin{aligned} \sigma_N &= |\mathbf{t}| \cos\{\theta\} \\ \tau &= |\mathbf{t}| \cos\{\beta\} \cos\{\phi\} \end{aligned} \quad (4.2)$$

where $|\mathbf{t}|$ is the magnitude of \mathbf{t} , θ is the angle between the habit plane normal and \mathbf{t} , β the angle between \mathbf{t} and the direction of the maximum resolved shear stress, and ϕ the angle between the latter and the direction of shear for the bainite plate concerned. A positive U means that the bainite variant is favoured by the applied stress and *vice versa*.

The experiments reported here are based on stress-affected transformation, *i.e.*, the external stress was kept below the yield strength of the austenite at the temperature

concerned. Plastic strain in the austenite can have other effects, for example the favouring of variants which grow across slip-planes and hence avoid mechanical stabilisation (Bokros and Parker, 1963; Durlu and Christian, 1979). Such effects become particularly prominent at large strains (Chatterjee et al., 2006) but might be neglected when the debris associated with plasticity is insufficient to hinder the progress of growing plates. For example, it has been shown that when an austenitic stainless steel is elongated by 10% and then transformed to martensite, the resulting crystallographic texture can be calculated using the variant selection criterion inherent in equation 4.2, (Kundu and Bhadeshia, 2006).

5. Data

The transformation texture can in principle be calculated from a knowledge of the initial texture of the polycrystalline austenite, and by taking into account variant selection due to applied stress (Kundu and Bhadeshia, 2006). But in doing so, it is important to realise that the shape deformation, habit plane and orientation relationship of any particular plate of bainite are mathematically connected by the crystallographic theory (Bowles and MacKenzie, 1954; Wechsler et al., 1953). A complete set of crystallographic data is therefore necessary before rigorous calculations can be attempted. Unfortunately, such data are frequently not available, so one purpose of the present work was to study the sensitivity of the texture predictions relative to the crystallographic inputs and the accuracy of routinely available experimental techniques.

The set of data designated (i) in Table 1 refer those used (Kundu and Bhadeshia, 2006) to model the martensitic transformation texture in an austenitic stainless steel, but adapted using the theory described in (Bhadeshia, 2001b) for the lattice parameters of interest in the present work, *i.e.*, $a_\gamma = 0.3619$ nm and $a_\alpha = 0.2882$ nm (Hase et al., 2004). This results in a macroscopic transformation-strain which is a shear of 0.2292 and a dilatational strain of 0.01 normal to the habit plane. The maximum fraction of bainite possible in the alloy system studied, for a transformation temperature of 300°C, is 0.63. The austenite is therefore never allowed in the calculations to transform to a fraction of bainite greater than this.

The analysis that follows assumes the first set of data listed in Table 1 to describe the displacive transformation to bainite. The remaining data will be discussed towards the end of the paper to illustrate the sensitivity of the calculations to crystallographic characteristics.

6. Strains due to Transformation

It is instructive to examine the strains that develop when bainite forms in a polycrystalline sample of austenite (γ), under the influence of a uniaxial stress.

The relationship between the sample and crystal frames of reference can be described using Euler angles ϕ_1 , ϕ and ϕ_2 . These are the three angles by which the sample reference frame must be rotated in order to coincide with that of the crystal. The rotation matrix relating the frames is given by:

$$\begin{pmatrix} \cos\phi_1\cos\phi_2 - \sin\phi_1\cos\phi\sin\phi_2 & \sin\phi_1\cos\phi_2 + \cos\phi_1\cos\phi\sin\phi_2 & \sin\phi\sin\phi_2 \\ -\cos\phi_1\sin\phi_2 - \sin\phi_1\cos\phi\cos\phi_2 & -\sin\phi_1\sin\phi_2 + \cos\phi_1\cos\phi\cos\phi_2 & \sin\phi\cos\phi_2 \\ \sin\phi_1\sin\phi & -\cos\phi_1\sin\phi & \cos\phi \end{pmatrix} \quad (6.1)$$

To generate a random set of austenite grains, the angles ϕ_1 and ϕ_2 (ranging from 0-2 π) and the value of $\cos\phi$ (between ± 1) are selected using a random number generator (Bunge, 1982). To simulate a polycrystalline state, a set of 500 austenite grains were assembled, each identified by a rotation matrix relating it to the sample frame.

Table 1. Sets of crystallographic data. The first set was used by Kundu and Bhadeshia (2006) to successfully estimate the martensitic transformation texture of austenitic stainless steel, but adjusted for the lattice parameters relevant here – the habit plane is close to $\{2\ 9\ 5\}_\gamma$. Although there are no complete data available for the bainitic steel analysed in the present work, the first set is the most appropriate given the approximate habit plane recently reported for the same steel by Zhang and Kelly (2006). The other two sets correspond to what are conventionally referred to as (ii) $\{2\ 5\ 2\}_\gamma$ (Dunne and Wayman, 1971a), and (iii) $\{3\ 15\ 10\}_\gamma$ (Dunne and Wayman, 1971b; Ledbetter and Wayman, 1971) habits. Each set describes the features of a single plate. γ and α refer to austenite and bainite respectively.

	Habit plane \mathbf{p}_γ	Shape change (γ P γ)
(i)	$\begin{pmatrix} -0.168640 \\ -0.760394 \\ -0.627185 \end{pmatrix}$	$\begin{pmatrix} 0.992654 & -0.033124 & -0.027321 \\ 0.026378 & 1.118936 & 0.098100 \\ -0.027321 & -0.123190 & 0.898391 \end{pmatrix}$
(ii)	$\begin{pmatrix} 0.362929 \\ 0.853900 \\ 0.373011 \end{pmatrix}$	$\begin{pmatrix} 0.986887 & -0.030853 & -0.013478 \\ 0.040751 & 1.095879 & 0.041883 \\ -0.051772 & -0.121809 & 0.946790 \end{pmatrix}$
(iii)	$\begin{pmatrix} -0.169270 \\ -0.761321 \\ -0.625890 \end{pmatrix}$	$\begin{pmatrix} 0.992602 & -0.033274 & -0.027355 \\ 0.026503 & 1.119202 & 0.097997 \\ -0.027355 & -0.123033 & 0.898853 \end{pmatrix}$
Orientation (γ J α)		
(i)		$\begin{pmatrix} 0.575191 & 0.542067 & 0.097283 \\ -0.550660 & 0.568276 & 0.089338 \\ -0.008610 & -0.131800 & 0.785302 \end{pmatrix}$
		$[\bar{1}\ 0\ 1]_\gamma [-0.920611\ -1.062637\ 1.084959]_{\alpha'}$ $(1\ 1\ 1)_\gamma (0.015921\ 0.978543\ 0.971923)_{\alpha'}$
(ii)		$\begin{pmatrix} 0.584634 & 0.519305 & 0.119189 \\ -0.529661 & 0.583719 & 0.059597 \\ -0.046858 & -0.118861 & 0.813418 \end{pmatrix}$
		$[\bar{1}\ 0\ 1]_\gamma [-1.011144\ -1.021828\ 1.021817]_{\alpha'}$ $(1\ 1\ 1)_\gamma (0.008115\ 0.984163\ 0.992204)_{\alpha'}$
(iii)		$\begin{pmatrix} 0.575371 & 0.542097 & 0.097510 \\ -0.550726 & 0.568476 & 0.089244 \\ -0.008855 & -0.131888 & 0.785465 \end{pmatrix}$
		$[\bar{1}\ 0\ 1]_\gamma [-0.920868\ -1.062349\ 1.084370]_{\alpha'}$ $(1\ 1\ 1)_\gamma (0.015790\ 0.978685\ 0.972219)_{\alpha'}$

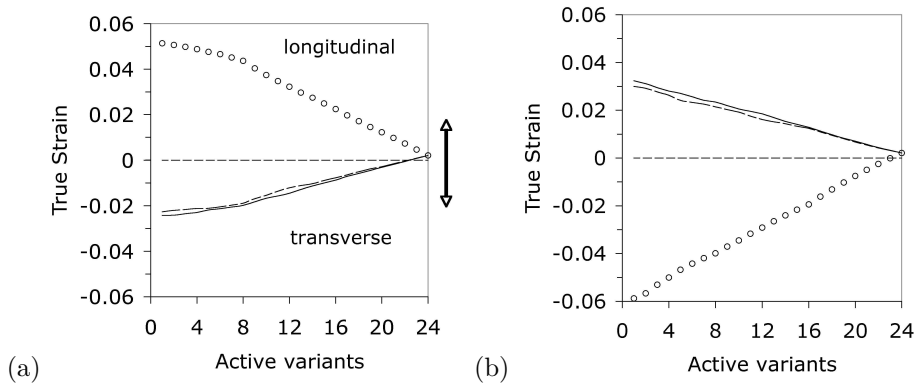


Figure 2. Strains developed due to transformation along the $[1\ 0\ 0]_S$ direction (labelled longitudinal, along the stress axis), and the transverse directions $[0\ 1\ 0]_S$ and $[0\ 0\ 1]_S$. (a) Tensile stress. (b) Compressive stress.

The three sample axes are henceforth referred to as $[1\ 0\ 0]_S$, $[0\ 1\ 0]_S$ and $[0\ 0\ 1]_S$, where “S” is the basis symbol and it may be assumed that the stress is applied along $[1\ 0\ 0]_S$. The true strains are then calculated by examining how unit vectors along the sample basis vectors are stretched due to transformation. The true strain in each case is $\ln\{|\mathbf{v}|/|\mathbf{u}|\}$. Notice that the strains need not be isotropic when variant selection occurs (Bhadeshia et al., 1991; Magee, 1970; Matsuzaki et al., 1994).

Equation 4.2 was used to determine the interaction energy U of each bainite plate with the applied stress; the variants were then ranked in descending order of U . The transformation strain was then calculated for all 24 cases within a given austenite grain, beginning with the most favoured variant consuming the maximum fraction of austenite permitted – this fraction is 0.63 for the specific experiments analysed here (Hase et al., 2004). Subsequent calculations assumed groups of most favoured variants forming in equal fractions up to the maximum allowed. The results are presented in Fig 2 for uniaxial tension and compression.

The true strain along $[1\ 0\ 0]_S$ is different between tension and compression mostly because the natural logarithm function scales the ratio of the initial to final length of $[1\ 0\ 0]_S$ differently depending on whether the ratio is greater or less than one. However, some difference is expected because unlike tension, the positive dilatational strain opposes compression. When all 24 possible variants are allowed to form, the shear strains essentially cancel, so both cases lead to an almost isotropic expansion, Fig 2a and b. However, when variant selection occurs, none of the three directions show equal strain.

It is interesting to analyse the effect of prior austenite texture on transformation plasticity.

The γ -textures studied are commonly described as the Goss $\{1\ 1\ 0\} \langle 0\ 0\ 1 \rangle_\gamma$, Cube $\{1\ 0\ 0\} \langle 0\ 0\ 1 \rangle_\gamma$ and Copper $\{1\ 1\ 2\} \langle 1\ 1\ \bar{1} \rangle_\gamma$ varieties (Dilamore and Roberts, 1965; Raabe, 2003; Tanaka, 1981). The first austenite grain is then aligned to the sample axes, for example in the Goss scenario, as follows:

$$[1\ 1\ 0]_\gamma \parallel [0\ 0\ 1]_S \quad [0\ 0\ 1]_\gamma \parallel [1\ 0\ 0]_S$$

Another 499 grains are then generated by randomly choosing rotation axes, but limiting the right-handed angle of rotation to the range $0\text{--}45^\circ$ to avoid a random distribution.

Fig. 3 shows the longitudinal strain along $[1\ 0\ 0]_S$ when a polycrystalline sample of austenite undergoes displacive transformation under the influence of a uniaxial tensile stress applied along the same direction. The results show that the observed longitudi-

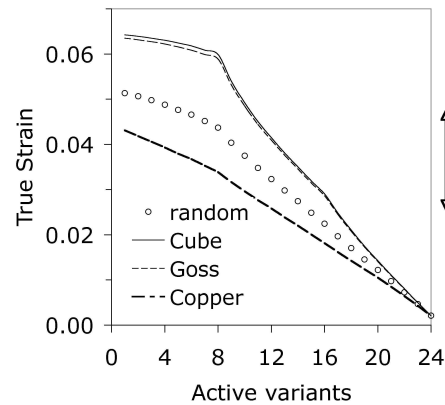


Figure 3. The longitudinal strain along $[1\ 0\ 0]_S$ when a polycrystalline sample of austenite undergoes displacive transformation (Table 1) under the influence of a uniaxial tensile stress. There are four different austenite textures represented, random, Goss, Cube and Copper.

nal strain can be greater or less than that expected from the transformation of random austenite, depending on the exact nature of the crystallographic texture and of course, the orientation of the stress axis. Naturally, all the results converge when the number of active variants per grain is large since the shear terms then cancel.

(a) *Multiaxial Stresses*

The cases considered above deal with uniaxial stress – there exist circumstances, for example when conducting welding, in which combinations of stresses are imposed during transformation. The system is then represented by a stress tensor σ_{ij} and the traction \mathbf{t} on any plane is then given in the usual way by the product of the tensor with the unit normal \mathbf{h} to the plane concerned. The traction can then be resolved into a normal and shear stress on the plane. The axes of the stress tensor correspond to those of the sample.

For a pure shear, $\sigma_{11} = -\sigma_{33}$ with all the other components of the tensor being zero. Fig. 4a shows the strains that develop in a random polycrystalline sample of austenite subjected to pure shear. The anisotropy of strain is pronounced, with the minimum strain naturally along the $[0\ 1\ 0]_S$ direction. Notice that unlike ordinary plastic deformation, the strain along $[0\ 1\ 0]_S$ is non-zero. This is because the basic unit of deformation is not shear, but an invariant-plane strain with a finite volume change δ directed normal to the habit plane.

The case for hydrostatic compression ($\sigma_{11} = \sigma_{22} = \sigma_{33} < 0$) is illustrated in Fig. 4b. The shear component of the invariant-plane strain does not in this case interact with the pressure, so the only contribution to the transformation strain is from δ . This explains why the strains are about an order of magnitude smaller. However, the individual strains are still anisotropic since the volume expansion is directed normal to the habit plane of each plate.

Having constructed the model, we now proceed to use it to interpret some specific experimental data on bainite. Whereas the measured transformation strains are from published work (Hase et al., 2004), the crystallographic measurements are new.

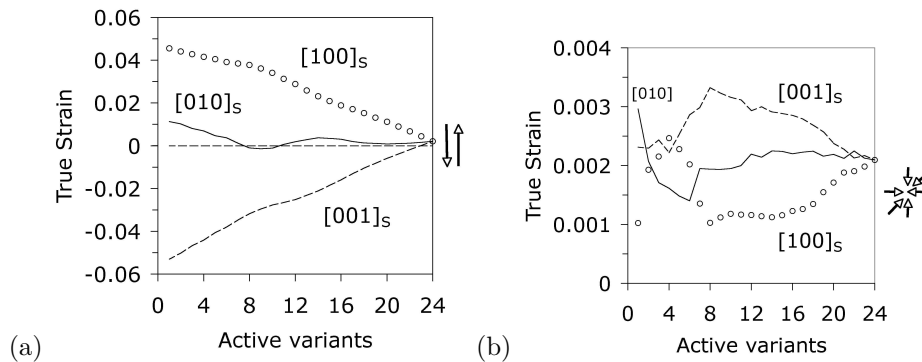


Figure 4. (a) Transformation strain when the specimen is subjected to pure shear. (b) The case for hydrostatic compression.

Table 2. Chemical composition, wt% of the bainitic steel studied.

C	Si	Mn	P	Al	Mo	Cr	Co
0.79	1.56	1.98	0.002	1.01	0.24	1.01	1.51

7. Experimental Procedure

The steel studied is from recent work involving the generation of extremely fine plates of bainite by transformation at unusually low temperatures (Bhadeshia, 2005b; Caballero and Bhadeshia, 2005; Hase et al., 2006). This has the advantage that larger stresses can be applied to influence transformation before the onset of ordinary plastic deformation in the austenite. The results therefore truly refer to stress-affected rather than strain-induced transformation. The chemical composition of the steel is given in Table 2.

The alloy was homogenised at 1200°C for 48 h. Small cylindrical specimens 10 mm diameter and 12 mm height were prepared for use in a thermo-mechanical simulator *Thermecmaster Z*. In the simulator, the samples were induction heated under vacuum (4.0×10^{-2} Pa) to 900°C and held at that temperature for 1800 s for austenitisation. They were then cooled at 25°C s^{-1} to 300°C using helium gas. A uniaxial compressive stress of 200 MPa was applied as soon as the sample reached 300°C, prior to any transformation.

The specimens were then held isothermally at 300°C for 4 h while monitoring the dimensional change in the radial direction using a laser transducer. The specimens were later studied metallographically on their longitudinal sections, and subjected to electron backscattered diffraction (EBSD) in a Hitachi S-4300 scanning electron microscope with a resolution of 0.05 μm with a step size of 0.25 μm .

8. Comparison with Experiments: Variant selection

Fig. 5 is an orientation image of a sample transformed to bainite under the influence of a uniaxial compressive stress. The colours represent crystallographic orientation using a standard technique called electron backscatter diffraction (EBSD) (Dingley and Nowell, 2004; Humphreys, 2004). The rectangles mark particular grains of austenite which were subjected to detailed analysis.

The crystallographic data from the EBSD analysis can be represented on stereographic projections in two common ways, by plotting the raw poles or by using pole-density contours on the projections. Both methods are used here for illustrative purposes.

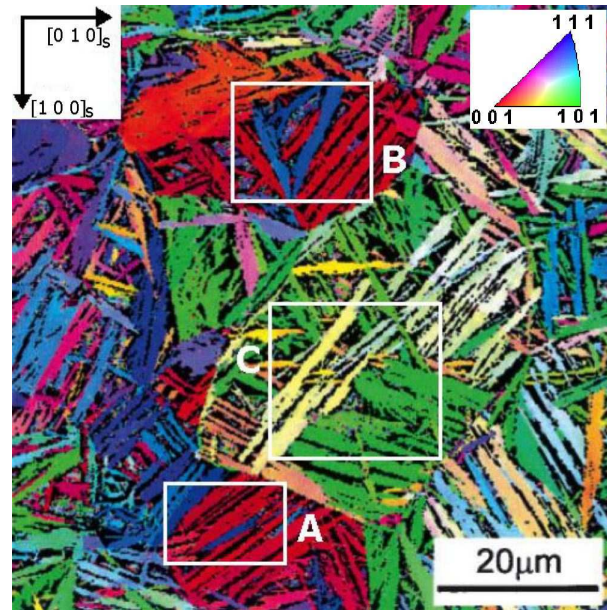


Figure 5. Orientation image. The colours represent different crystallographic orientations.

Considering the autesnite in grain A first, the $1\ 0\ 0_{\gamma}$ pole figure is shown in Fig. 6a,b. There is a clear spread in the orientation of the austenite grain, presumably due to strains caused by transformation. It is well known that the formation of bainite introduces dislocation debris in the adjacent austenite (Bhadeshia and Edmonds, 1979; Swallow and Bhadeshia, 1996). The plotting of pole-density contours somewhat exaggerates the spread in orientation, as can be seen by comparing Fig. 6a,c with Fig. 6b,d. This is because a 5° Gaussian spread was applied around the orientations.

Table 3 lists the interaction energies between the bainite variants and the applied stress, with a positive energy denoting a favourable interaction. There are, therefore, 12 favoured variants, within which the first eight are in a class of high values of U with the remainder with much smaller positive interaction energies.

It is clear from Fig. 6e, which compares experimental versus calculated data, that allowing the eight most favoured variants explains the major intensities in the experimental data. Allowing all 12 of the favoured variants (Fig. 6f) completes the match between the calculated data, and all positions on the stereogram where measured intensity exists. It is interesting that the addition of a further four favoured variants with lower values of U in Fig. 6f explains the residual lowest-intensity components of the experimental data.

Fig. 7 shows reasonable agreement between the experimental data and calculations for grain B. The high intensity areas designated 'H' correspond to the eight most favoured variants, whereas those designated 'L' are of lower intensity and are explained by the next four less favoured variants listed in Table 3. This confirms that the strongest intensities observed correspond to the most favoured variants.

Grain B happens to be roughly in Goss orientation relative to the sample axes. For this orientation, a different transformation texture has been demonstrated both by measurement and by calculation when martensite is induced by *tensile deformation* (Gey et al., 2005; Kundu and Bhadeshia, 2006), compared with that illustrated in Fig. 7c,d. To explain this, the transformation textures were calculated for both compression (consistent with the present experiments) and tension, for an austenite grain in the exact Goss orientation.

Table 3. Interaction energy U (J mol^{-1}) for a uniaxial compressive stress of magnitude 200 MPa, for each of the 24 possible variants of bainite in grain A of austenite. The energies are arranged in descending order, with positive values corresponding to a favourable interaction with the applied stress and vice versa.

Grain A	151.2	144.2	133.4	124.6	111.6	111.1	95.7	93.9
	35.6	26.7	24.4	15.7	-7.8	-7.8	-10.9	-12.2
	-126.8	-131.7	-139.0	-145.1	-147.3	-148.8	-152.8	-153.0
Grain B	152.2	151.8	150.4	149.8	143.5	142.9	141.4	141.0
	12.8	12.8	10.9	10.7	10.5	10.3	8.4	8.4
	-167.0	-167.3	-168.8	-169.3	-173.9	-174.5	-175.9	-176.3
Grain C	139.6	128.0	95.4	73.1	71.8	65.9	64.6	64.0
	63.2	38.9	4.1	0.9	-4.8	-21.1	-40.0	-40.5
	-64.1	-83.7	-96.1	-98.6	-110.1	-119.3	-119.8	-126.7

The results are illustrated in Fig. 8a,b which shows that both the tensile (Gey et al., 2005; Kundu and Bhadeshia, 2006) and compression data can be explained by the present model by assuming the formation of all twelve of the favoured variants.

The result from grain C needs special discussion – the interaction energies are again listed in Table 3. A maximum of twelve favoured variants can form, but it is not possible to explain all of the observed intensity using the 12 variants for which $U > 0$, Fig. 9. There are some low-intensity regions which are not explained. These discrepancies indicate additional variants which are not favoured by the applied stress. Fig. 9 confirms that the low-intensity regions correspond to the two variants with interaction energies of -2.5 and -10.5 J mol^{-1} , *i.e.*, the unfavourable variants with the least interaction with the applied stress.

The formation of unfavourable variants with low interaction energies is easy to understand when it is realised that at the transformation temperature of 300°C, the chemical free energy change is about -1225 J mol^{-1} (Hase et al., 2004), a value much greater than the magnitude of U . This chemical driving force can therefore stimulate transformation even though it opposes the applied stress.

9. Comparison with Experiments: Transformation Strain

Measured radial strains due to isothermal transformation to bainite under the influence of a stress are illustrated in Fig. 10 (Hase et al., 2004). The maximum transverse strain at 200 MPa is 0.017 and that at 4 MPa is 0.004. The latter value of strain is consistent with an approximately random texture in the polycrystalline austenite, because $3 \times$ radial-strain corresponds to the expected volume strain for the observed extent of transformation. The values of stress essentially correspond to transformation greatly influenced by stress and not affected, respectively. The strain data are macroscopic measurements made on polycrystalline samples of austenite. The data are therefore simulated by considering a cluster of 500 randomly oriented austenite grains, each of which makes a contribution to the overall strain during transformation.

The interaction energy for each of the 24 bainite variants, in each of the 500 austenite grains, was calculated. The data were then arranged in descending order for each grain (as in Table 3). Of course, the most favoured variants and indeed the values of U will be different for each grain as a function of its orientation. But it then becomes possible to pick the n most favoured variants from each of the 500 descending arrays of U . Fig. 11 shows the calculated transverse strains to be expected when a number n of the most favoured variants form in each of the 500 austenite grains.

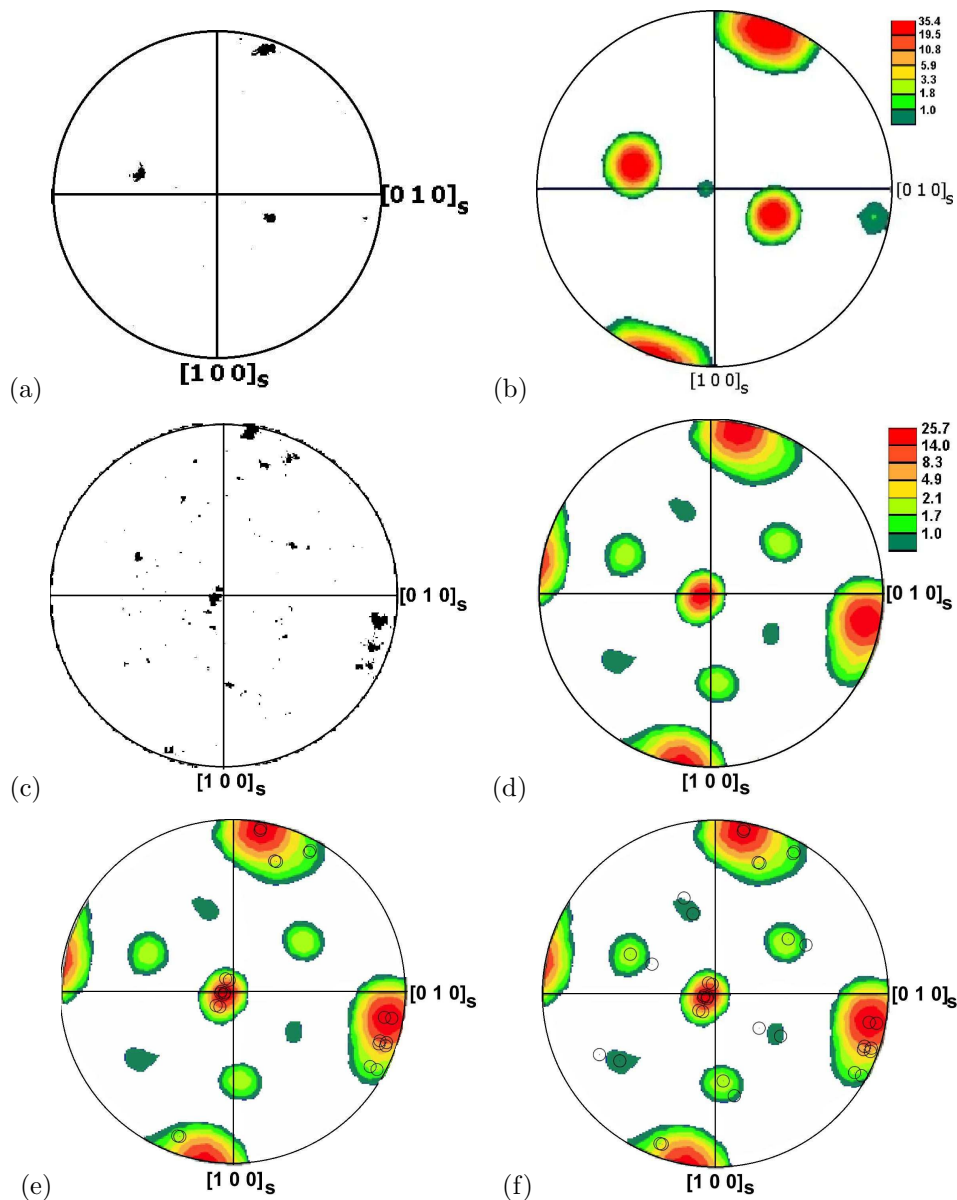


Figure 6. Pole figures for grain A, relative to the sample frame of reference. (a,b) $1\ 0\ 0_\gamma$ pole figures, (c,d) $1\ 0\ 0_\alpha$ pole figures. (e) Comparison with calculated $1\ 0\ 0_\alpha$ pole figures, allowing the 8 most favoured variants to form. (f) Comparison with calculated $1\ 0\ 0_\alpha$ pole figures, allowing the 12 most favoured variants to form.

It is evident that the observed strains can be explained if it is assumed that between 12–14 of the most favoured variants form when transformation occurs under the influence of a large stress. By contrast, in the absence of a significant stress, it is necessary to assume that most variants form, *i.e.*, there is almost no variant selection. This is consistent with the crystallographic observations described earlier.

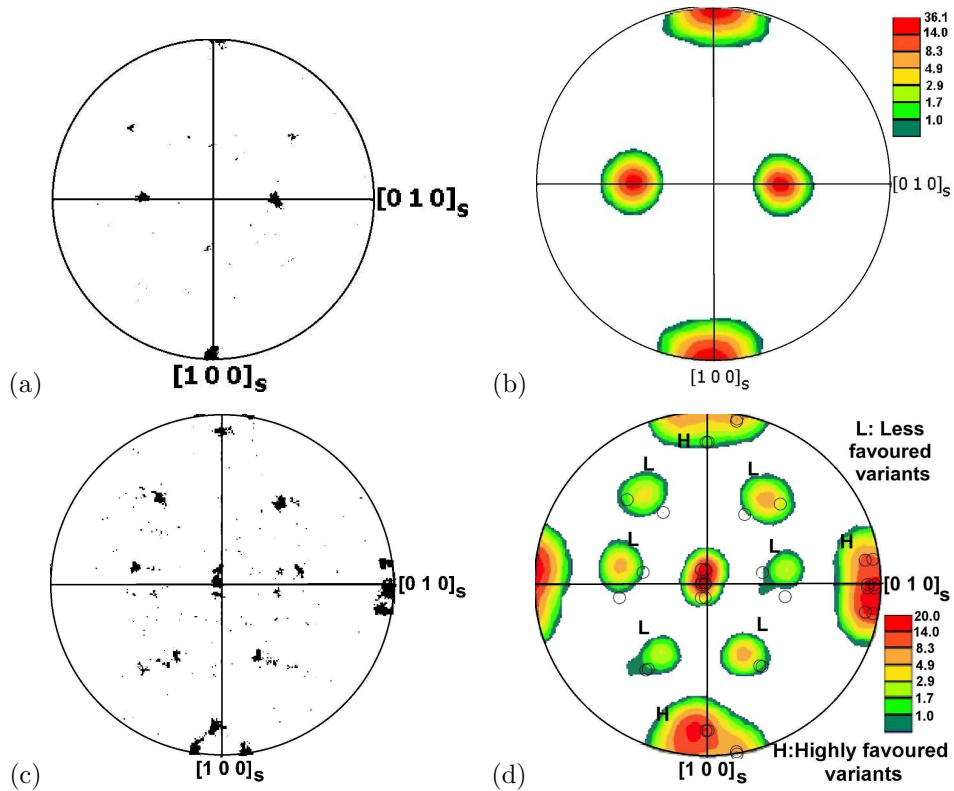


Figure 7. Pole figures for grain B, relative to the sample frame of reference. (a,b) $1\ 0\ 0_\gamma$ pole figures, (c) $1\ 0\ 0_\alpha$ pole figure. (d) $1\ 0\ 0_\alpha$ pole figure with calculated data superimposed.

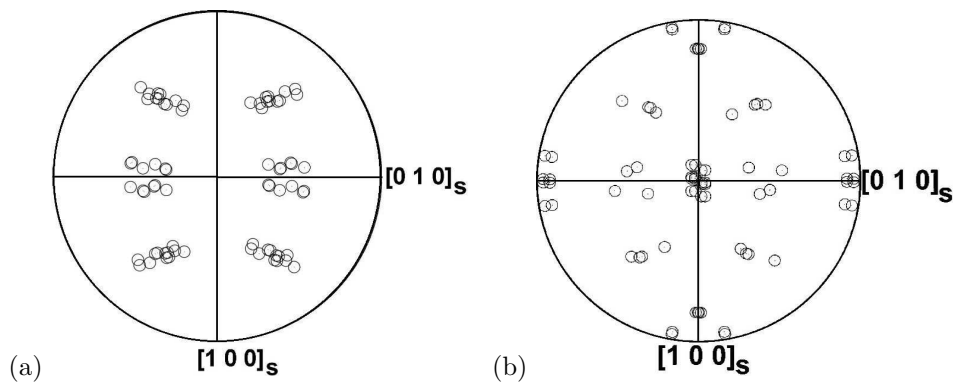


Figure 8. Calculated $1\ 0\ 0_{\alpha'}$ pole figures relative to the sample frame of reference, showing the twelve most favoured variants of bainite. (a) Tensile and (b) compressive uniaxial stress. In this figure poles are allowed to form from both hemispheres.

However, the analysis leaves open the question of the degree of variant selection as a function of the magnitude of the applied stress. This is tackled next.

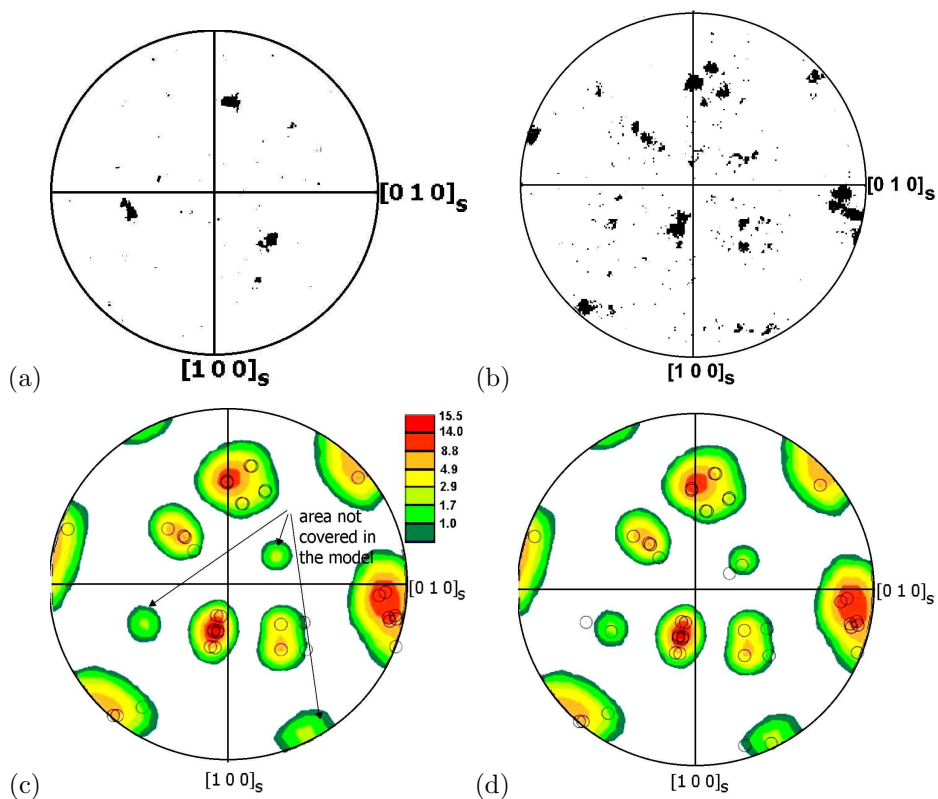


Figure 9. Pole figures for grain C, relative to the sample frame of reference. (a) $1\ 0\ 0_\gamma$ pole figures, (b) $1\ 0\ 0_\alpha$ pole figure. (c) $1\ 0\ 0_\alpha$ pole figure with calculated data superimposed for the 12 most favoured variants. (d) $1\ 0\ 0_\alpha$ pole figure with calculated data superimposed for the 14 most favoured variants.

(a) *Extent of Variant Selection versus Stress*

The total free energy available for transformation is the sum of chemical and mechanical components, the latter being zero in the absence of an applied stress during transformation:

$$\Delta G = \Delta G_{CHEM} + \Delta G_{MECH} \quad (9.1)$$

It would be reasonable to assume that there is strong variant selection when the ratio of $\Delta G_{MECH}/\Delta G$ is large. Given relevant dilatometric data, the extent of variant selection can be determined as in Fig. 11. The chemical free energy can readily be calculated using standard methods, here done using MTDATA (Chart et al., 1975). The mechanical free energy change depends on the particular variant in a given austenite grain and on the orientation of that grain in the sample frame. Calculations were done for all 24 variants in each austenite grain, for all 500 austenite grains. The maximum value found for each austenite grain was then averaged over all the 500 austenite grains.

Table 4 was compiled using data from the published literature. The data cover a pressure vessel steel (Bhadeshia et al., 1991), a low-temperature bainitic steel (Hase et al., 2004) and a high-silicon steel (Matsuzaki et al., 1994).

It is evident from Fig. 12 that there is a strong linear correlation between the ratio $\Delta G_{MECH}/\Delta G$ and the number of most favoured variants allowed to form in each of the

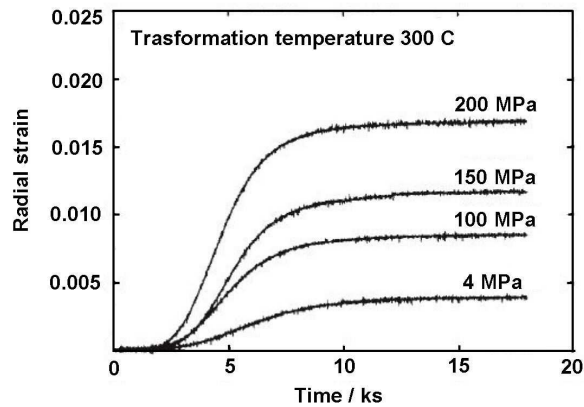


Figure 10. Radial strain for isothermal transformation at 300°C as a function of compressive stress (Hase et al., 2004).

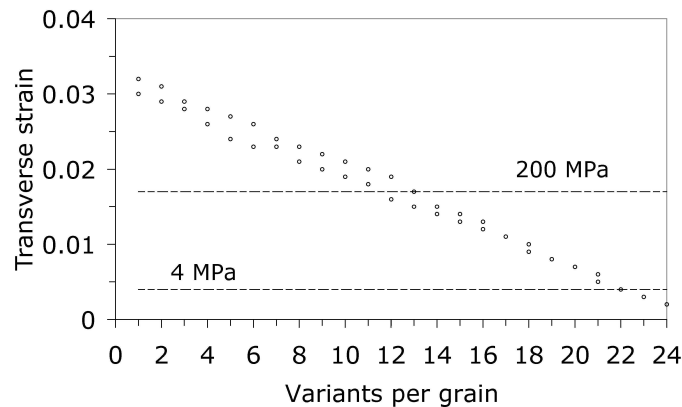


Figure 11. Radial strains for isothermal transformation at 300°C as a function of the number of most favoured variants allowed in each of 500 austenite grains. The measured strains are plotted as horizontal lines.

austenite grains. This is an important observation in that it allows for the first time the extent of variant selection, and hence the transformation strains, to be calculated as a function of stress for any steel.

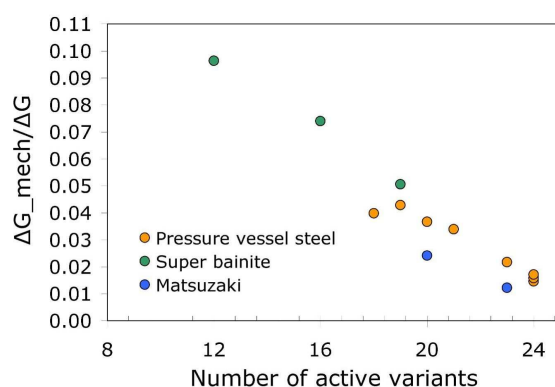
10. Stress-free Transformation from Textured Austenite

In their classic work on the stress-free transformation to bainite, Davenport and Bain in 1930 (Davenport and Bain, 1930) noticed that “the volume change (due to transformation) is not necessarily uniformly reflected in linear change in all dimensions”. They even found that the thickness of a flat disc specimen actually decreased as the volume increased! Bhadeshia *et al.* found a similar effect and explained it qualitatively in terms of transformation from textured austenite (Bhadeshia et al., 1991).

Fig. 13 shows calculated strains along three orthogonal directions for a cluster of

Table 4. Calculated data for a variety of steels. T is the transformation temperature and σ is the stress.

Reference	$T / ^\circ\text{C}$	σ / MPa	$U / \text{J mol}^{-1}$	$\Delta G_{\text{CHEM}} / \text{J mol}^{-1}$	n	$\frac{\Delta G_{\text{MECH}}}{\Delta G}$
Bhadeshia <i>et. al.</i> Bhadeshia <i>et al.</i> (1991)	400	98.4	61.84	1758	21	0.017
“	420	98.4	61.75	1620	20	0.019
“	440	98.4	61.67	1486	18	0.020
“	460	96.5	60.67	1354	19	0.022
“	400	41.5	26.08	1758	24	0.007
“	420	41.6	26.11	1620	24	0.008
“	440	41.4	25.95	1486	24	0.009
“	460	47.8	30.05	1354	23	0.011
Hase <i>et. al.</i> Hase <i>et al.</i> (2004)	300	-200	130.62	1225	12	0.051
“	300	-150	97.97	1225	16	0.038
“	300	-100	65.31	1225	19	0.026
Matsuzaki <i>et. al.</i> Matsuzaki <i>et al.</i> (1994)	450	-25	29.69	1199	23	0.006
“	450	-50	14.84	1199	20	0.012

Figure 12. $\Delta G_{\text{MECH}}/\Delta G$ versus the number of most favoured variants per grain (n), for a variety of steels.

100 austenite grains with a Cube texture which transform to bainite, as a function of the number of variants that form. It is evident that the model is capable of explaining Davenport and Bain's observations if the number of variants that form in the textured austenite is limited, for example because the special grain boundaries present in such austenite limit the variants of bainite that can nucleate.

11. Sensitivity to Crystallographic Data

It is a fact that detailed crystallographic data of the kind listed in Table 1 are few and far between. However, a large number of ferrous alloys fall roughly within the range of the three sets in Table 1 (Bhadeshia, 2001a; Dunne and Wayman, 1971b). It is instructive therefore to analyse the sensitivity of the calculated texture to the data. Fig. 14 shows the analysis for grain B. A comparison of the stereograms shows that the texture is reasonably predicted for all three sets, although there are detailed differences for the $\{2\ 5\ 2\}_\gamma$. These

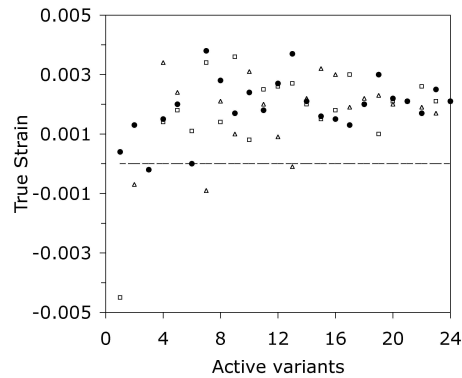


Figure 13. Longitudinal (filled circles) and transverse strains observed when Cube textured austenite transforms into bainite without the influence of externally applied stress.

differences are important if the accuracy of the experimental technique is greater. Large numbers of accurate measurements can indeed be made, as demonstrated by Nolze (2004) with respect to the orientation relationship between the austenite and martensite but such accuracy is not common, particularly when EBSD measurements are reported. There also is a need for complete crystallographic measurements of the shape deformation, habit plane and orientation relationship of the transformation products in the new steels.

12. Conclusions

A theory has been compiled for calculating both the macroscopic strains and crystallographic texture which develop when apolycrystalline sample of austenite is transformed into bainite or martensite under the influence of applied stress or a system of stresses. Indeed, the theory can be applied to any scenario where the shape deformation due to displacive transformation is defined.

Any texture present in the austenite prior to transformation can also be taken into account. Comparisons with experimental data on a bainitic steel are encouraging. There are also detailed outcomes, such as the consequences on transformation texture due to a reversal of sign in the applied stress, which have not previously been highlighted.

One of the most interesting outcomes is that a strong correlation has been obtained between the proportion of the driving force attributed to stress, and the extent of variant selection. The correlation is entirely expected when it is considered that the driving force has both chemical and mechanical origins, and hence can be used quantitatively to estimate transformation plasticity.

13. Acknowledgments

The authors are grateful to the EPSRC, Tata Steel (India) and JFE Steel Corporation (Japan) for funding this work.

References

Bhadeshia, H. K. D. H., 2001a. *Bainite in Steels*, 2nd edition. Institute of Materials, London.

Proceedings of The Royal Society A, 463 (2007) 2309-2328.

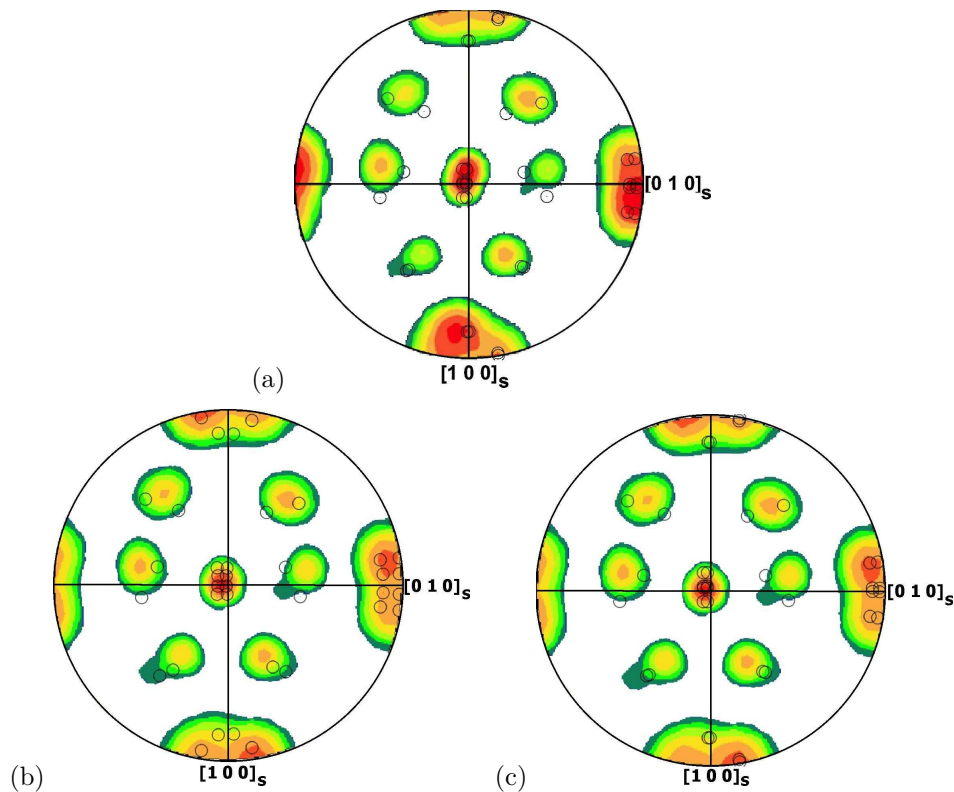


Figure 14. $1\ 0\ 0_\alpha$ pole figures for grain B, assuming crystallographic data corresponding to the following approximate habit planes (Table 1): (a) $\{2\ 9\ 5\}_\gamma$ (reproduced from Fig. 7d), (b) $\{2\ 5\ 2\}_\gamma$, (c) $\{3\ 15\ 10\}_\gamma$.

Bhadeshia, H. K. D. H., 2001b. *Geometry of Crystals*. 2nd edition, Institute of Materials.

Bhadeshia, H. K. D. H., 2005a. Developments in martensitic and bainitic steels: Role of the shape deformation. *Materials Science and Engineering A* 378, 34–39.

Bhadeshia, H. K. D. H., 2005b. Large chunks of very strong steel. *Materials Science and Technology* 21, 1293–1302.

Bhadeshia, H. K. D. H., David, S. A., Vitek, J. M., Reed, R. W., 1991. Stress induced transformation to bainite in a Fe-Cr-Mo-C pressure vessel steel. *Materials Science and Technology* 7, 686–698.

Bhadeshia, H. K. D. H., Edmonds, D. V., 1979. The bainite transformation in a silicon steel. *Metallurgical Transactions A* 10A, 895–907.

Bokros, J. C., Parker, E. R., 1963. The mechanism of the martensite burst transformation in Fe-Ni single crystals. *Acta Metallurgica* 11, 1291–1301.

Bowles, J. S., MacKenzie, J. K., 1954. The crystallography of martensite transformations. *Acta Metallurgica* 2, 129–137.

Bunge, B. J., 1982. *Mathematische Methoden der Texturanalyse*. Butterworth, London.

Proceedings of The Royal Society A, 463 (2007) 2309–2328.

- Caballero, F. G., Bhadeshia, H. K. D. H., 2005. Very strong bainite. *Current Opinion in Solid State and Materials Science* 8, 186–193.
- Chart, T. G., Counsell, J. F., Jones, G. P., Slough, W., and Spencer, P. J. Provision and use of thermodynamic data for the solution of practical problems. *International Metals Reviews*, 20, 57–82.
- Chatterjee, S., Wang, H. S., Yang, J. R., Bhadeshia, H. K. D. H., 2006. Mechanical stabilisation of austenite. *Materials Science and Technology* 22, 641–644.
- Davenport, E. S., Bain, E. C., 1930. Transformation of austenite at constant subcritical temperatures. *Trans. Am. Inst. Min. Metall. Engng.* 90, 117–154.
- Dilamore, I. L., Roberts, W. T., 1965. Preferred orientation in wrought and annealed metals. *Metallurgical Reviews* 10, 271–380.
- Dingley, D. J., Nowell, M. M., 2004. The use of electron backscatter diffraction for the investigation of nano crystalline materials and the move towards orientation imaging in the TEM. *Microchimica Acta* 147, 157–165.
- Dunne, D. P., Wayman, C. M., 1971a. An assessment of the double shear theory as applied to ferrous martensitic transformations. *Acta Metallurgica* 19, 425–438.
- Dunne, D. P., Wayman, C. M., 1971b. The crystallography of ferrous martensite. *Metallurgical Transactions* 2, 2327–2341.
- Durlu, T. N., Christian, J. W., 1979. Effect of prior deformation on the martensite burst transformation in single crystals of an Fe-Ni-C alloy. *Acta Metallurgica* 27, 663–666.
- Eckerlid, J., Nilsson, T., Karlsson, L., 2003. Fatigue properties of longitudinal attachments welded using low transformation temperature filler. *Science and Technology of Welding and Joining* 8, 353–359.
- Gey, N., Petit, B., Humbert, M., 2005. Electron backscattered diffraction study of martensitic variants induced by plastic deformation in 304 stainless steel. *Metallurgical & Materials Transactions* 36, 3291–3299.
- Hase, K., Garcia-Mateo, C., Bhadeshia, H. K. D. H., 2006. Bimodal size-distribution of bainite plates. *Materials Science and Engineering A* A438–440, 145–148.
- Hase, K., Mateo, C. G., Bhadeshia, H. K. D. H., 2004. Bainite formation influenced by large stress. *Materials Science and Technology* 20, 1499–1505.
- Humphreys, F. J., 2004. Characterisation of fine-scale microstructures by electron backscatter diffraction (EBSD). *Scripta Materialia* 51, 771–776.
- Ko, T., Cottrell, S. A., 1952. The formation of bainite. *Journal of the Iron and Steel Institute* 172, 307–313.
- Kundu, S., Bhadeshia, H. K. D. H., 2006. Transformation texture in deformed stainless steel. *Scripta Materialia* 55, 779–781.
- Ledbetter, H. M., Wayman, C. M., 1971. A computer program for martensite crystallography. *Materials Science and Engineering* 7, 151–157.
- Magee, C. L., 1970. The nucleation of martensite. In: Aaronson, H. I., Zackay, V. F. (Eds.), *Phase Transformations*. ASM, Metals Park, Ohio, USA, pp. 115–156.

- Matsuzaki, A., Bhadeshia, H. K. D. H., Harada, H., 1994. Stress-affected bainitic transformation in a Fe-C-Si-Mn alloy. *Acta Metallurgica and Materialia* 42, 1081–1090.
- Nolze, G., 2004. Characterisation of the fcc/bcc orientation relationship by EBSD using pole figures and variants. *Zietschrift für Metallkunde* 95, 744–755.
- Ohta, A., Matsuoka, K., Nguyen, N. T., Maeda, Y., Suzuki, N., 2003. Fatigue strength improvement of lap welded joints of thin steel plate using low transformation temperature welding wire. *Welding Journal, Research Supplement* 82, 77s–83s.
- Ohta, A., Suzuki, N., Maeda, Y., Hiraoka, K., Nakamura, T., 1999a. Superior fatigue crack growth properties in newly developed weld metal. *International Journal of Fatigue* 21, S113–S118.
- Ohta, A., Watanabe, O., Matsuoka, K., Shiga, C., Nishijima, S., Maeda, Y., Suzuki, N., Kubo, T., 1999b. Fatigue strength improvement by using newly developed low transformation temperature welding material. *Welding in the World* 43, 38–42.
- Patel, J. R., Cohen, M., 1953. Criterion for the action of applied stress in the martensitic transformation. *Acta Metallurgica* 1, 531–538.
- Raabe, D., 2003. Overview of basic types of hot rolling textures of steels. *Steel Research International* 74, 327–337.
- Swallow, E., Bhadeshia, H. K. D. H., 1996. High resolution observations of displacements caused by bainitic transformation. *Materials Science and Technology* 12, 121–125.
- Tanaka, T., 1981. Controlled rolling of steel plate and strip. *International Metals Reviews* 4, 185–212.
- Timoshenko, S. P., Goodier, J. N., 1982. *Theory of Elasticity*. McGraw Hill International Book Company, London.
- Wechsler, M. S., Lieberman, D. S., Read, T. A., 1953. On the theory of the formation of martensite. *Trans. AIME Journal of Metals* 197, 1503–1515.
- Zhang, M.-X., Kelly, P. M., 2006. Crystallography of carbide-free bainite in a hard bainitic steel. *Materials Science and Engineering A* A438–440, 272–275.